Wiley Online Library
Early View publication on www.wileyonlinelibrary.com
(issue and page numbers not yet assigned;
citable using Digital Object Identifier – DOI)

Phys. Status Solidi C, 1600262 (2017) / DOI 10.1002/pssc.201600262

physica status solidi pss c
www.pss-c.com
current topics in solid state physics

The doping mechanism and electrical performance of polyethylenimine-doped MoS_2 transistor

Seongin Hong[1], Geonwook Yoo[2], Dong Hak Kim[1], Won Geun Song[1], Ong Kim Le[3], Young Ki Hong[1], Kaito Takahashi[4], Inturu Omkaram[*,1], Do Ngoc Son[**,3], and Sunkook Kim[*,1]**

[1] Multi-Functional Nano/Bio Lab., Sungkyunkwan University, Gyeonggi 16419, South Korea
[2] School of Electronic Engineering, Soongsil University, Seoul 06978, Korea
[3] Ho Chi Minh City University of Technology, VNU-HCM, 268 Ly Thuong Kiet Street, District 10, Ho Chi Minh City, Vietnam
[4] Institute of Atomic and Molecular Sciences, Academia Sinica, No. 1, Roosevelt Road, Section 4, P. O. Box 23-166, Taipei 10617, Taiwan, ROC

Received 20 December 2016, accepted 14 February 2017
Published online 10 March 2017

Keywords multilayer MoS_2, n-doping, optoelectronic device, PEI, transistor

* Corresponding author: e-mail kimskcnt@gmail.com
** e-mail ngocson.do@gmail.com, Phone: +84(0)902 243 265, Fax: +84(0)838 3863 5869
*** e-mail omkar_inturu@yahoo.com

We present a systematic investigation of polyethylenimine (PEI) doping mechanism and its effects on the multilayer MoS_2 field effect transistors (FETs). The threshold voltages of MoS_2 FETs before (i.e., pristine) and PEI doping are observed at 3.7 and 0.72 V, respectively. This negative threshold voltage shift clearly reveals that the PEI molecules effectively act as n-type dopants. The electrical properties are improved by absorption of PEI molecules onto MoS_2 channel because the width of Schottky barrier (SB) is narrowed by the induced interfacial dipole between PEI molecules and MoS_2 layers. Through the density function theory (DFT) calculation and X-ray photoelectron spectroscopy (XPS) analysis, we confirm that formation of Mo–N bond generates new energy state into the bandgap. Consequently, the hole carriers can easily tunnel through the barrier under negative gate voltage. Furthermore, PEI doping improve photoresponsivity and time-resolved photo-switching characteristics because of the new energy state. Our studies demonstrate the PEI doping method has a great potential for improving electrical and optical properties of MoS_2-based devices.

© 2017 WILEY-VCH Verlag GmbH & Co. KGaA, Weinheim

1 Introduction Over the past few years, the substitution of host atoms with dopants as practiced in two-dimensional (2D) transition-metal dichalcogenides (TMDCs) has been researched due to potential applications in various electronic [1–3], optoelectronic [4], and spintronic [5] devices. Namely, the incorporation of dopants in TMDCs layers like MoS_2 films results in the n- and p-type conductivities that are necessary to form p–n junctions which are fundamental units in modern electronic-integrated circuits. However, the TMDC materials are lacking in selective doping of the traditional semiconductor technologies that allows the exploration of novel approaches, such as chemical and molecular doping. Chemical doping has been used to investigate the surface charge transfer between dopant molecules and TMDCs layers [6–9] which modulates the Fermi level and thus results in the modification of the optical and electrical properties of 2D materials. The physisorbed O_2, and H_2O molecules [6] electronically depleted n-type materials such as MoS_2 and $MoSe_2$ and Lin et al. [10] reported nondegenerate n-doping of MoS_2 using cesium carbonate (CS_2CO_3). P atoms from phosphorus silicate glass (PSG) enabled uniform n-type doping in MoS_2, which is essential in realizing integrated circuit based on 2-D materials [11]. The n-type doping effect increased the electron density in the chemical-doped 2-D-layered materials, resulting in the

© 2017 WILEY-VCH Verlag GmbH & Co. KGaA, Weinheim

shift of the Fermi level toward the conduction band edge. In contrast, the energy level in the region of the valence band after benzyl viologen (BV) doping can turn monolayer MoS_2 into n-type semiconductor similar to the organic molecule functionalized BN sheets [12].

Otherwise, the techniques in n- and p-type doping based on polymers, such as polyethylenimine (PEI), with different dipole moments were reported by Du et al. [13] and Li et al. [14]. For example, electrical characteristics of MoS_2 FETs show that fluoroalkyl trichlorosane – SAMs with a large positive dipole moment significantly reduce the intrinsic n-type characteristics of MoS_2 flakes (p-type doping), where 3-(trimethoxysilyl)-1 propanamine SAMs improve the intrinsic n-type characteristics (n-type doping) [14]. Lithium fluoride (LiF) is a widely used n-type dopant for the organic semiconductor due to its strong electron-donating ability which results in large reduction in contact resistances [15]. Such n-type doping phenomenon can be associated with the formation of dipoles that eventually increase tunneling of electrons from a source metal to MoS_2 via reduced Schottky barrier (SB) width.

In this paper, we reported the n-type doping of MoS_2 FETs using PEI molecules. After PEI doping, we observed to modulation of SB width due to interfacial dipoles between PEI molecules and MoS_2 layers. We confirmed that amine groups in PEI molecules induced new states in the bandgap using density functional theory (DFT) and X-ray photoelectron spectroscopy (XPS) measurement. Furthermore, in order to show the potential of PEI-doped MoS_2 FETs in optoelectronic application, we performed optical power-dependent and time-resolved photo-response measurements.

2 Experimental Multilayer MoS_2 flakes were prepared by using mechanical exfoliation method from bulk MoS_2 crystal (SPI crystals) on a heavily doped p-type Si substrate with a 300-nm-thick thermal SiO_2. After MoS_2 flakes were transferred onto the SiO_2/Si substrate, we fabricated back-gated multilayer MoS_2 field effect transistors (FETs) with the channel length (15.34 μm) and width (24.90 μm) as shown in Fig. 1(a). The source and drain electrodes were patterned by conventional photolithography. Ti/Au (20/100 nm) electrodes were deposited using e-beam evaporator. To improve electrical properties of the multilayer MoS_2 FETs, the transistor was annealed in a furnace at 300 °C in N_2 ambient. Then we drop-casted polyethylenimine (PEI) solution, as shown in Fig. 1(b), onto the multilayer MoS_2 FETs for a certain time (5, 10, 30, and 60 min) to immerse MoS_2 channel, and then rinsed to remove PEI solution for 90 s in deionized (DI) water. Figure 1(b) shows a schematic of PEI-doped MoS_2 FETs. The electrical properties of both pristine and PEI-doped MoS_2 FETs were measured using Keithley 4200 semiconductor parameter analyzer at room temperature in ambient condition.

3 Results and discussion The electrical characteristics of the as-fabricated devices exhibit a typical transfer characteristic of n-channel FET. The transistor has unipolar current dominated by electron conduction. In Fig. 2(a), transfer curves (I_{ds} vs. V_{gs} for $V_{ds} = 1$ V) of the pristine and PEI-doped MoS_2 FETs are compared. Due to the excellent n-channel behavior, the transfer characteristics show that the devices have good electrical performance with a high I_{on}/I_{off} ratio of $\sim 10^6$. Here, the threshold voltage (V_{th}) for a MoS_2 transistor is extracted by the linear extrapolation method from the drain current measured as a function of gate voltage. Before doping, the MoS_2 transistor exhibits V_{th} of 3.7 V, but the V_{th} shifted to 0.72 V after PEI doping as shown in Fig 2(a) inset. The negative shift of V_{th} induced by PEI doping confirms that the PEI molecules on MoS_2 FETs strongly act as n-type dopants. The transfer characteristics of a back-gated MoS_2 FET device before doping has an ON current of ~ 3.3 μA, but the ON current with PEI doping increases to ~ 4.8 μA in MoS_2 FETs for a 45% enhancement. Furthermore, the output characteristics of the representative pristine and doped PEI are depicted in Fig. 2(b), where I_{ds} in a low field regime of V_{ds} linearly increased with V_{ds}. At higher V_{ds}, I_{ds} for MoS_2 FETs gradually saturates at $V_{gs}–V_{th} = 40$ V in high field region. The improvement in I_{ds} of the PEI-doped device in comparison to the pristine is mainly attribute to the increased channel conductance by PEI molecular dipole induced SB width reduction.

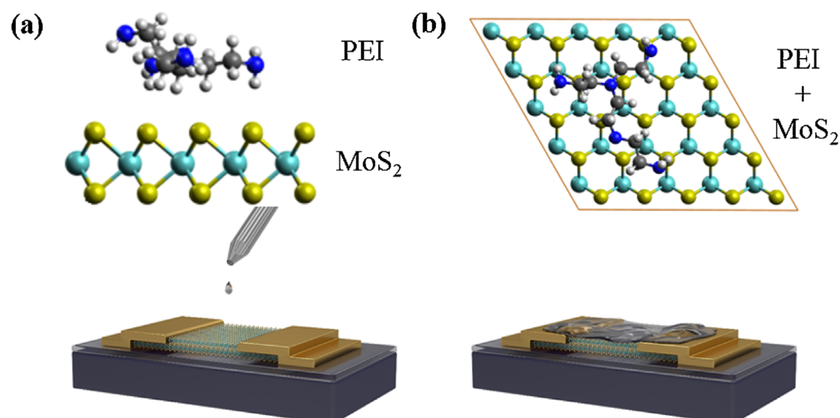

Figure 1 (a) Structure of MoS_2 and the truncated-branched PEI molecules. The PEI molecules were doped by using drop casting method on the multilayer MoS_2 back-gate FETs. (b) Schematic view of the PEI-doped multilayer MoS_2 back gate FETs. The most favorable adsorption configuration of the PEI molecule on the MoS_2 multilayer.

© 2017 WILEY-VCH Verlag GmbH & Co. KGaA, Weinheim

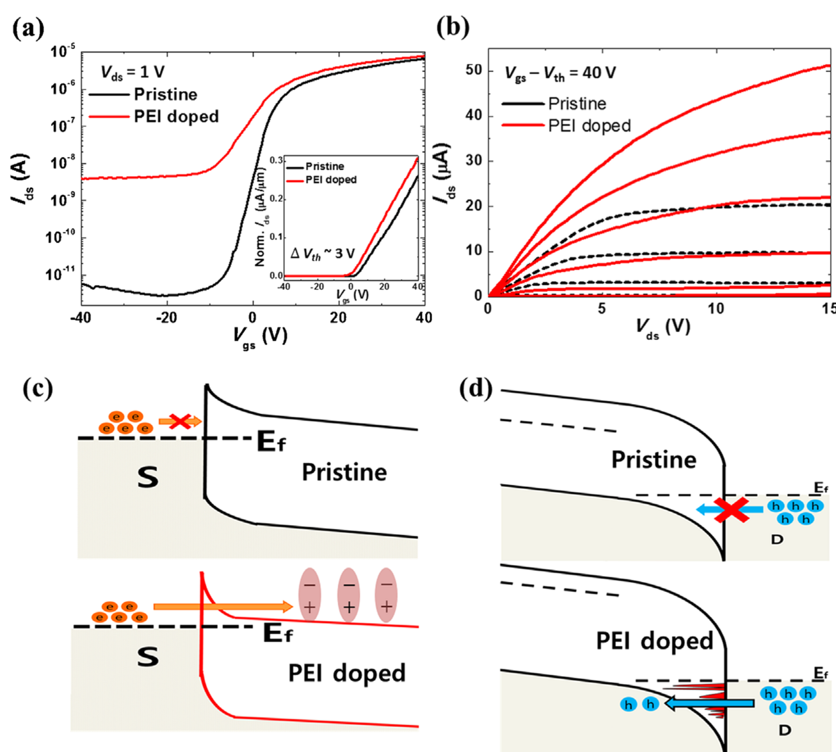

Figure 2 (a) Transfer *I–V* and (b) output characteristics of the pristine and PEI-doped multilayer back-gate MoS_2 FETs. The inset of (a) shows the V_{th} shift (−3.02 V) and the currents normalized to the device width ($W = 24.90$ μm). Schematic energy band diagram of (c) ON current region ($V_{gs} > 0$) and (d) OFF current region ($V_{gs} < 0$).

To investigate the in-depth of carrier transport with PEI doping on MoS_2 surface, Fig. 2(c) and (d) showed the proposed energy band diagrams in ON and OFF regimes, respectively. In the pristine MoS_2 FET, SB at the Ti-MoS_2 can hinder carrier injection from source electrodes to MoS_2 channel. Here amine groups in PEI molecules absorbed on the surface of MoS_2 has the property of the positively interface dipoles. The positive dipoles at interface of PEI/MoS_2 created excess carriers in the channel, which forms quasi-Fermi level (E_{Fn}) close to the conduction band (E_c). The quasi-Fermi level formed after PEI doping results in the reduction of the SB width, and thus electrons can more efficiently tunnel through the reduced Schottky barrier as explained in Fig. 2(c). The MoS_2 energy band move downward due to positively charged dipoles, which increases the electric field at the source-MoS_2 junction by enhancing the tunneling of electrons and causes the negative V_{th} shift. Therefore, the SB width at the Ti-MoS_2 can be modulated with respect to the PEI doping method, and the contact resistance could be lowered with increasing PEI molecules [13]. Furthermore, the increased OFF can be ascribed to charge transfer from the amine groups of PEI to MoS_2 introduced by the presence of new states created near the binding energy edge of the valence band. The appearance of the new states in the PEI-doped MoS_2 suggests that the electronic interactions may enhance the charge transfer by creating unoccupied states near the Fermi level. New valance states within the bandgap eventually make it easier for holes to tunnel through the barrier from drain metal to MoS_2 (hole carriers – Fig. 2(d)). Under negative V_{gs}, the transport of hole carriers from drain to MoS_2 is negligible but the new states in junction of MoS2/drain electrode increase the OFF current. The adsorption of the PEI molecules onto the MoS_2 can improve electrical properties of the MoS_2 FET, which will be consistent with DFT calculation.

In order to understand the effects of PEI doping on the electronic structure of MoS_2, we calculated the band structure of monolayer MoS_2 before and after the adsorption of PEI molecules. The calculation was performed using the DFT within a plane-wave basis set, which was implemented in the Vienna *ab initio* simulation package (VASP) [16]. Band structure of the monolayer MoS_2 is presented in Fig. 3 (a). The monolayer MoS_2 has a direct bandgap of 1.75 eV at the *K* point in the Brillouin zone, which agrees with the previous reports [17–20]. The electronic density of state (DOS) shows that the valence band maximum and the conduction band minimum are contributed mainly by Mo 4d states and weakly by S 3p states. As shown in Fig. 3(b), however, the adsorption of PEI molecules creates new energy levels near the valence band. The new energy levels in the region of valence band can contribute to new current paths in OFF regime as the PEI molecules were absorbed. Similar results could be found from the literature for organic molecules [10]. The new flat energy levels are mainly attributed to the N 2p lone pairs.

To confirm the PEI doping mechanism, XPS measurements were performed on the surface of both pristine and PEI-doped MoS_2. Figure 3(c) shows Mo 3d and S 2p core level spectra of the pristine MoS_2 flakes. The Mo $3d_{5/2}$ and Mo $3d_{3/2}$ peaks of the pristine MoS_2 were observed around 229.8 and 232.9 eV, respectively, separated by about 3.1 eV.

 © 2017 WILEY-VCH Verlag GmbH & Co. KGaA, Weinheim

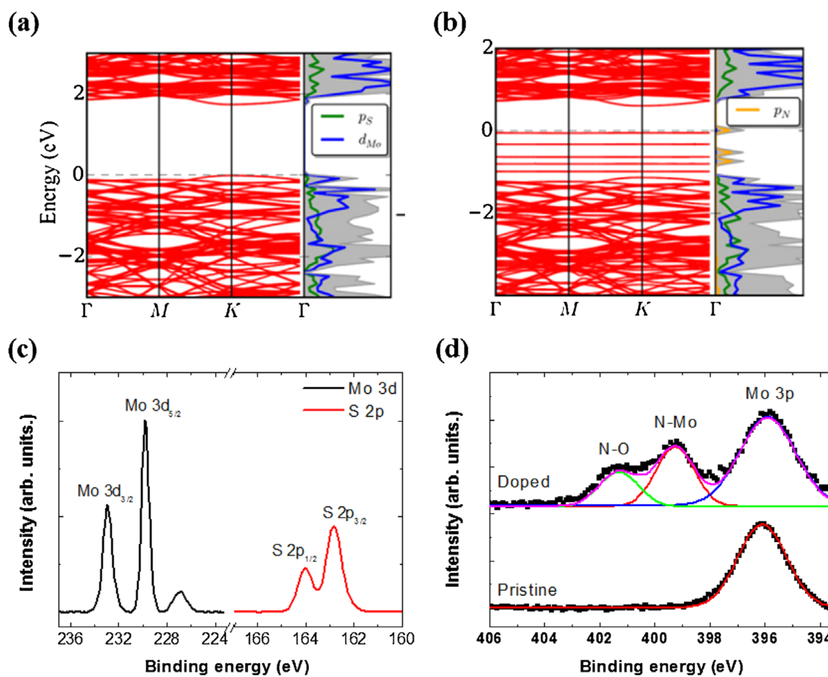

Figure 3 Band structure and DOS of the monolayer MoS_2: (a) the pristine and (b) adsorption of the PEI molecule. Gray-shaded area is the total electronic density of state. The Fermi level is set at 0 eV. XPS spectra of the (c) Mo 3d, S2p and (d) N 1s core levels measured from pristine and PEI-doped MoS_2.

In addition, the S 2p peaks were observed at 162.8 and 164.0 eV corresponding to S $2p_{1/2}$ and S $2p_{3/2}$, respectively. Figure 3(d) clearly shows the formation of Mo-N bonding in the PEI-doped MoS_2 from the XPS analysis of the N 1s core level. The Mo $3p_{3/2}$, Mo-N, and N-O peaks of the PEI-doped MoS_2 were observed at 395.5, 397.5, and 401.3 eV, respectively. On the contrary, we could only observe Mo $3p_{3/2}$ peak in the pristine MoS_2. So, it was convinced that nitrogen atoms from the amine group of PEI molecules were absorbed and formed Mo–N bond. The XPS analysis corresponds to our DFT calculation results. Thus, the DFT calculation and XPS analysis clearly indicate that MoS_2 layers were successfully doped using the PEI molecules with nitrogen lone pair electrons affecting electrical properties.

In addition, the multilayer MoS_2 FETs could also be used as photodetector due to their remarkable optical absorption property [21, 22]. In order to characterize and compare photoresponse properties of the pristine and PEI-doped MoS_2 FETs, we performed I_{ds}-V_{gs} measurements under various incident laser power densities from 0.2 to 3.2 mW cm^{-2} at a wavelength of 785 nm and $V_{ds} = 1$ V as shown in Fig. 4(a) and (b). The photoresponsivity could be extracted using the following equation:

$$R = I_{ph}/(P_{inc}S),$$

where $I_{ph}(= I_{total} - I_{dark})$ is the photo-induced photocurrent, S is the channel area of the device, and $P_{inc}\left(W/cm^2\right) = P_{tot}/A_{laser}$ (A_{laser} is the area of laser spot) is the incident power density. The photoresponsivity of the pristine MoS_2 was $\sim 1.37 \times 10^{-1}$ A W^{-1} at $V_{gs} = -40$ V and 0.2 mW. However, the PEI doping enhanced the photo-responsivity about $\sim$4.41 A W^{-1}. In the previous report [23, 24] that trap sites between the conduction band and valence band could improve the optical properties of TMDC materials. Similarly, our DFT calculation shows that the sub-gap states were generated into the bandgap after PEI doping, as shown Fig. 3(b), which could explain the strong improvement of the photoresponsivity. Figure 4(c) compared the photoswitching behaviors of the pristine and PEI-doped MoS_2 FETs measured from the time-resolved photoresponse. The time-resolved drain current of the pristine and the PEI-doped MoS_2 FETs was measured at $V_{gs} = 0$ V and $V_{ds} = 1$ V with a 405-nm wavelength laser. The incident laser was switched on and off with a power 0.1 mW and period 20 s, the time-resolved drain current responded immediately both the pristine and the PEI-doped MoS_2 FETs. Compare to the pristine MoS_2 FETs, the time-resolved drain current greatly increased about $\sim$30 times after PEI doping. As mentioned above, the photo-induced carrier density of PEI-doped MoS_2 was increased due to reduction of Schottky barrier width [25, 26]. After PEI doping on MoS_2, PEI molecules generate new energy sites within bandgap as mentioned DFT simulation. Thus, when the light is irradiated on the PEI-doped MoS_2 device, the partial holes of photo-generated electron–hole pairs are trapped in new energy level. Such trapped holes in new energy level can lead to band-bending in energy band diagram. Therefore, the enhanced photoresponsivity and photo-switching characteristic of the PEI-doped MoS_2 FETs demonstrate the device for potential application as optoelectronics.

4 Conclusions In this work, we have investigated the PEI doping mechanism and its effects on electrical and optical properties of multilayer MoS_2 FETs. Our DFT calculation and XPS measurement confirm that the PEI

© 2017 WILEY-VCH Verlag GmbH & Co. KGaA, Weinheim

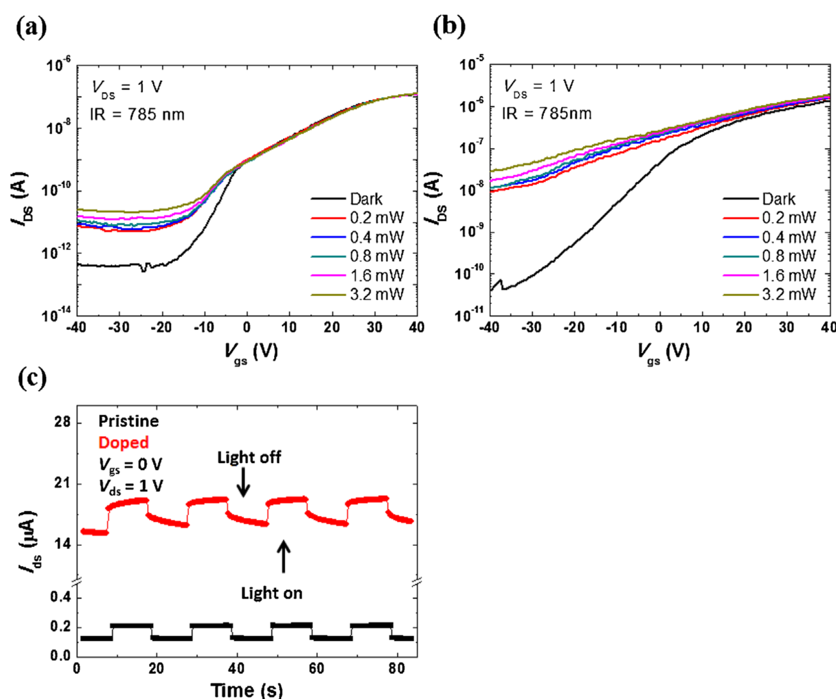

Figure 4 Transfer curves of (a) the pristine and (b) PEI-doped MoS_2 under illumination at various incident optical power densities with a wavelength of 785 nm. (c) The time-resolved photo-switching measurements of the PEI-doped MoS_2.

molecules were successfully doped and formed Mo–N bonds on the MoS_2 channel, generating new energy states near the valence band. The strong n-doping changed V_{th} as well as SB width attributed to the induced interfacial dipoles. Therefore, ON-current of the doped MoS_2 FETs were improved in comparison with the pristine. Furthermore, the PEI doping also enhanced photoresponsivity of the MoS_2 FETs from 0.14 to 4.41 A W^{-1}. Our in-depth study suggests that the PEI molecular doping could be widely applicable to the 2-D materials in order to improve electrical and optical properties.

Authors' contributions The paper was written through contributions of all authors. All authors have given approval to the final version of the paper. S. H. and G. Y. contributed equally to this work.

Notes The authors declare no competing financial interest.

Aknowledgements This research was supported in part by National Research Foundation of Korea (grant NRF-2015R1A1A1A05027488, NRF-2015R1A5A1037548, and NRF-2013M3C1A3059590) and in part by the Commercializations Promotion Agency for R&D Outcomes (COMPA) funded by the Ministry of Science, ICT and Future Planning (MISP).

References

[1] B. Radisavljevic, A. Radenovic, J. Brivio, V. Giacometti, and A. Kis, Nature Nanotechnol. **6**, 147–150 (2011).
[2] S. Kim, A. Konar, W. S. Hwang, J. H. Lee, J. Lee, J. Yang, C. Jung, H. Kim, J. B. Yoo, J. Y. Choi, Y. W. Jin, S. Y. Lee, D. Jena, W. Choi, and K. Kim, Nature Commun. **3**, 1011 (2012).
[3] J. S. Rhyee, J. Kwon, P. Dak, J. H. Kim, S. M. Kim, J. Park, Y. K. Hong, W. G. Song, I. Omkaram, M. A. Alam, and S. Kim, Adv. Mater. **28**, 2316–2321 (2016).
[4] Z. Yin, H. Li, H. Li, L. Jiang, Y. Shi, Y. Sun, G. Lu, Q. Zhang, X. Chen, and H. Zhang, ACS Nano **6**, 74–80 (2012).
[5] D. Xiao, G. B. Liu, W. Feng, X. Xu, and W. Yao, Phys. Rev. Lett. **108**, 196820 (2012).
[6] S. Tongay, J. Zhou, C. Ataca, J. Liu, J. S. Kang, T. S. Matthews, L. You, J. Li, J. C. Grossman, and J. Wu, Nano Lett. **13**, 2831–2836 (2013).
[7] S. Mouri, Y. Miyauchi, and K. Matsuda, Nano Lett. **13**, 5944–5948 (2013).
[8] J. Choi, H. Zhang, H. Du, and J. H. Choi, ACS Appl. Mater. Interfaces **8**, 8864–8869 (2016).
[9] N. H. Pour, Y. Anugrah, S. Wu, X. Xu and S. J. Koester, Device Research Conference (DRC). 2013 71st Annual, 101–102 (2013).
[10] J. D. Lin, C. Han, F. Wang, R. Wang, D. Xiang, S. Qin, X. A. Zhang, L. Wang, H. Zhang, A. T. Wee, and W. Chen, ACS Nano **8**, 5323–5329 (2014).
[11] H. Y. Park, M. H. Lim, J. Jeon, G. Yoo, D. H. Kang, S. K. Jang, M. H. Jeon, Y. Lee, J. H. Cho, G. Y. Yeom, W. S. Jung, J. Lee, S. Park, S. Lee, and J. H. Park, ACS Nano **9**, 2368–2376 (2015).
[12] Y. Jing, X. Tan, Z. Zhou, and P. W. Shen, J. Mater. Chem. A **2**, 16892–16897 (2014).
[13] Y. C. Du, H. Liu, A. T. Neal, M. W. Si, and P. D. Ye, IEEE Electron Device Lett. **34**, 1328–1330 (2013).
[14] Y. Li, C. Y. Xu, P. Hu, and L. Zhen, ACS Nano **7**, 7795–7804 (2013).
[15] H. M. Khalil, M. F. Khan, J. Eom, and H. Noh, ACS Appl. Mater. Interfaces **7**, 23589–23596 (2015).

© 2017 WILEY-VCH Verlag GmbH & Co. KGaA, Weinheim

[16] G. Kresse and J. Furthmüller, Phys. Rev. B **54**, 11169–11186 (1996).
[17] Y. G. Li, Y. L. Li, C. M. Araujo, W. Luo, and R. Ahuja, Catal. Sci. Technol. **3**, 2214–2220 (2013).
[18] A. Splendiani, L. Sun, Y. Zhang, T. Li, J. Kim, C. Y. Chim, G. Galli, and F. Wang, Nano Lett. **10**, 1271–1275 (2010).
[19] E. Scalise, M. Houssa, G. Pourtois, V. Afanas'ev, and A. Stesmans, Nano Res. **5**, 43–48 (2011).
[20] T. Li, Phys. Rev. B **85**, 235407 (2012).
[21] Q. H. Wang, K. Kalantar-Zadeh, A. Kis, J. N. Coleman, and M. S. Strano, Nat. Nanotech. **7**, 699–712 (2012).
[22] J. Kwon, Y. K. Hong, G. Han, I. Omkaram, W. Choi, S. Kim, and Y. Yoon, Adv. Mater. **27**, 2224–2230 (2015).
[23] S. Tongay, J. Suh, C. Ataca, W. Fan, A. Luce, J. S. Kang, J. Liu, C. Ko, R. Raghunathanan, J. Zhou, F. Ogletree, J. Li, J. C. Grossman, and J. Wu, Sci. Rep. **3**, 2657 (2013).
[24] C. Jung, S. M. Kim, H. Moon, G. Han, J. Kwon, Y. K. Hong, I. Omkaram, Y. Yoon, S. Kim, and J. Park, Sci. Rep. **5**, 15313 (2015).
[25] G. Haacke, J. Appl. Phys. **47**, 4086–4089 (1976).
[26] L. Romano, V. Privitera, and C. Jagadish, Defects in Semiconductors. Vol. **91**, (Academic Press, 2015).

© 2017 WILEY-VCH Verlag GmbH & Co. KGaA, Weinheim